# We are IntechOpen, the world's leading publisher of Open Access books
# Built by scientists, for scientists

**6,900**
Open access books available

**185,000**
International authors and editors

**200M**
Downloads

**154**
Countries delivered to

Our authors are among the

**TOP 1%**
most cited scientists

**12.2%**
Contributors from top 500 universities

CLARIVATE ANALYTICS
BOOK CITATION INDEX
INDEXED

**WEB OF SCIENCE**™

Selection of our books indexed in the Book Citation Index
in Web of Science™ Core Collection (BKCI)

## Interested in publishing with us?
## Contact book.department@intechopen.com

Numbers displayed above are based on latest data collected.
For more information visit www.intechopen.com

# Interactions Between Plasmonic Nanostructures and Proteins

Loredana Latterini and Luigi Tarpani

Additional information is available at the end of the chapter

## Abstract

In the development of a nanodevice for biomedical applications, the study of the interactions with the biomolecules is essential. Proteins, in particular, are known to be easily adsorbed on the surface of the nanoparticles and the resulting complex is the one that will be effectively internalized by the target cells. Owing to the versatility of the preparation methods available and the unique optical properties, gold nanomaterials represent an excellent choice to study this interaction. This chapter will initially describe the synthesis of gold nanorods and nanoshells that are able to absorb light in the near-infrared (NIR) region. Then, the methods available for the functionalization of their surface will be discussed. The surface plasmon absorption will be used as an optical tool to monitor the process of preparation and surface modification. In the last section of the chapter, fluorescence and microscopy techniques will be used to follow the formation and characterize the protein-nanoparticle complex. The modifications of the emission spectra of two model proteins, bovine serum albumin (BSA) and myoglobin (Mb), will be analyzed in detail. The data will demonstrate that structural rearrangements following the adsorption on the surface of the nanoparticles are responsible for the changes in the fluorescence of the tryptophan residues of the protein. The data will be discussed in terms of static and dynamic quenching, proving the formation of a protein-nanoparticle complex. Atomic force microscopy (AFM) measurements will allow the direct visualization of this complex.

**Keywords:** gold nanostructures, protein adsorption, localized surface plasmon resonance, fluorescence, atomic force microscopy

## 1. Introduction

In the last few decades, the use of nanotechnology in the biomedical field has grown exponentially. This interest is originated from the fact that materials at the nanometer scale have completely different properties than their bulk counterparts and these properties are dependent on the particle size [1, 2]. Also, nanoparticles are ideal systems for application in bioimaging and therapy because they are small enough to interact with the biomolecules and to be efficiently internalized by the cells.

The first and most important process that occurs when a nanoparticle comes in contact with a biological fluid is the association with proteins. In the design of engineered nanostructures, this process has to be taken into account, because it may determine the fate of these species inside the living cells, their clearance rate and cytotoxicity. In fact, the systems that will be eventually delivered to the final biological target are protein-coated nanoparticles and their surface properties will affect their ability to cross the cell membrane barrier. Also, the adsorption of proteins on the surface of the particles may lead to conformational changes, unfolding and eventually to their irreversible denaturation [3–5]. These processes could alter the normal protein functions and cause unwanted side-effects for the organism. For all these reasons, it is clear that a full comprehension of the nature and the mechanism of this process of association can be of support in the development of optimized nanostructures for biomedical applications.

Gold-based nanomaterials (GNMs) are among the most studied systems to be employed as diagnostic and therapeutic tools for biomedical applications. This success comes from their unique properties. They are highly biocompatible and the preparation method can be easily adjusted to control their morphology and optical properties. They also have easy processable surfaces, which allow the conjugation with different ligands for the specific targeting to the cells of interest. Most importantly, when gold is reduced to the nanometric size, the interaction with light under certain experimental conditions produces a strong absorption in the visible region caused by the collective oscillation of the electron cloud on the surface of the metal. This effect, known as localized surface plasmon resonance (LSPR), is extensively used in biological sensing and imaging [6–10]. In fact, the frequency at which LSPR occurs and its intensity are dependent on size and shape of the nanoparticles, interparticle distance and the dielectric function of the surrounding Medium. All these physical parameters can change upon interaction of the GNMs with the biological species. The adsorption of protein on GNMs drastically modifies the surface properties of gold colloids and may eventually lead to their aggregation. These effects result in changes in the LSPR optical response that can be measured by ultraviolet-visible (UV-Vis) spectroscopy.

Many other techniques are currently employed to study the interaction between proteins and nanoparticles, such as Fourier transform infrared spectroscopy (FTIR) [11, 12], nuclear magnetic resonance (NMR) [13], circular dichroism spectroscopy [12, 14], size-exclusion chromatography [15]. Among them, fluorescence is a powerful tool for probing the adsorption of proteins on the surface of nanoparticles because of its high sensibility in detecting even small changes in the microenvironment surrounding the emitting species. Additionally, the use of

the intrinsic fluorescence of the proteins to monitor the association process makes unnecessary the attachment of an imaging probe that may perturb the system under investigation.

In this chapter, the interaction of GNMs with different model proteins *in vitro* is analyzed by UV-Vis spectroscopy and microscopy techniques. The first section describes the most common methods of preparation of GNMs with the focus on those systems whose morphology promotes a shift of the LSPR in the NIR region. An efficient absorption of the system in this portion of the electromagnetic spectrum is desirable because the light at these energies has the maximum penetration in the biological tissues. This section also illustrates the synthetic steps able to functionalize the GNMs surface in order to tune the interaction with the proteins. In the second section, the detailed study of the adsorption of the model proteins on the surface of the GNMs is reported. The modifications of the protein structure and the formation of a complex with the GNMs are demonstrated by UV-Vis absorption and static and time-resolved fluorescence data. Atomic force microscopy (AFM) is used as complementary tool to characterize the protein-GNM complex.

## 2. Design of plasmonic GNMs

### 2.1. Nanorods

A class of GNMs, which has attracted much attention because of their potential as therapeutic agents in biomedicine, is gold nanorods (NRDs). They present two LSPR extinction bands, which correspond to the oscillation of the plasmons in the transversal and the longitudinal direction. The transversal mode is not strongly affected by the NRD morphology and the relative absorption occurs at about 520 nm. On the contrary, the position of the longitudinal LSPR can shift from the visible region to the NIR depending on the aspect ratio (length-to-width ratio). Higher is the aspect ratio, lower is the frequency at which the plasmon absorbs. In order to design NRDs with the desired optical properties, several computational methods have been developed to correlate the morphology of the NRDs with their absorption and scattering efficiencies [16–18] obtaining in most cases an excellent agreement between the simulations and the experimental data.

The first report of the synthesis of gold NRDs is from the group of Jana et al. in 2001 [19]. This experimental procedure is known as the seed-mediated growth method and it is still the most common preparation for this type of GNM. In this synthesis, gold nanoparticles of 1–3 nm (seeds) are obtained by reduction of a $Au^{3+}$ salt by $NaBH_4$ in the presence of a surfactant, usually sodium citrate or cetyltrimethylammonium bromide (CTAB), as stabilizer. These seeds are then quickly added to an aqueous growth solution containing $AgNO_3$, CTAB and $Au^+$ ions formed by partial reduction of $Au^{3+}$ with ascorbic acid. The seeds act as nucleation centers for the reduction of $Au^+$ to atomic gold and CTAB, which has a strong affinity for specific facets of the metal, promotes the anisotropic growth of the rod. Through this method, it is possible to obtain NRDs of about 15 nm wide and up to 100 nm long depending on the amount of $AgNO_3$ and the seed to gold molar ratio in the growth solution. NRDs with higher aspect ratio

presenting the longitudinal LSPR region can be still produced with this procedure by an additional growth step in the presence of a mixture of two surfactants [20].

The extinction spectra and the corresponding transmission electron microscopy (TEM) images of two samples of NRDs synthesized by our group using the seed-mediated growth method are shown in **Figure 1**. The sample (a), having an aspect ratio of 2.3 ± 0.2 as determined by the analysis of the TEM images, presents an intense longitudinal LSPR absorption band centered at 652 nm. The use of a larger amount of silver ions in the growth solution increases the NRDs aspect ratio to 4.8 ± 0.2, which shifts the longitudinal band to 775 nm (**Figure 1**, sample b).
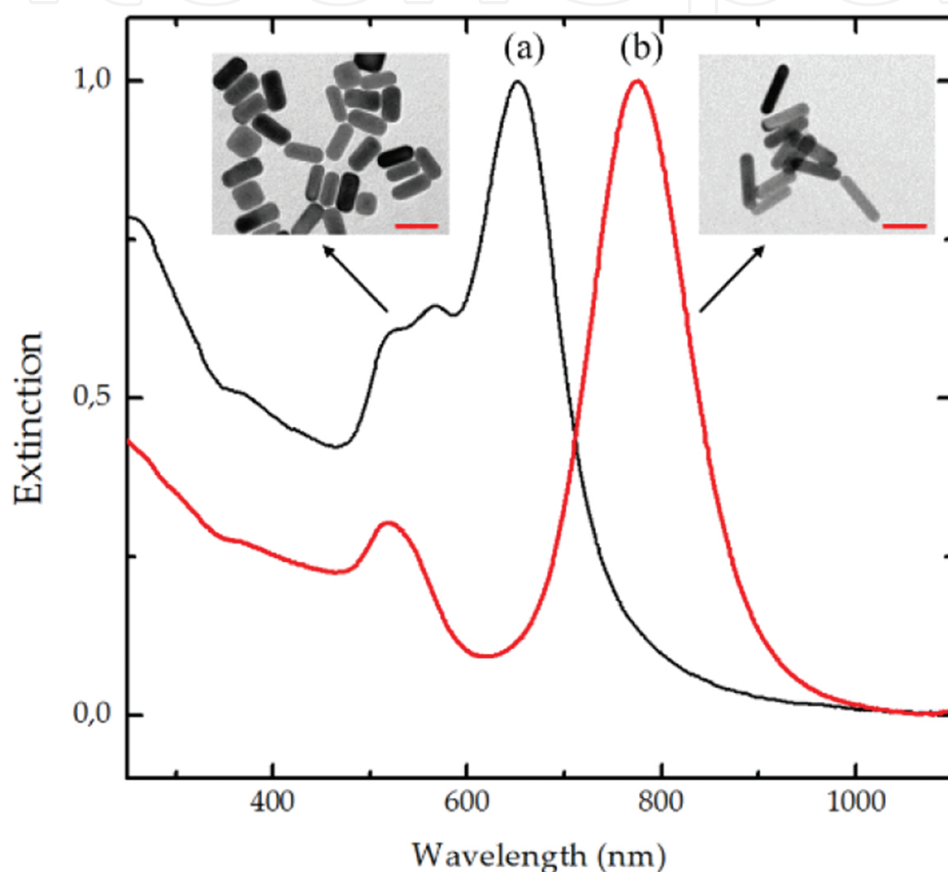


**Figure 1.** Extinction spectra of NRDs with an aspect ratio of 2.3 (a) and 4.8 (b) and the corresponding TEM images (scale bar = 50 nm). An increase in the amount of silver ions added in solution allows the formation of nanorods with a higher aspect ratio and with an extinction spectra shifted at longer wavelengths.

## 2.2. Nanoshells

An interesting approach to shift the LSPR absorption in the NIR region is the synthesis of gold nanoshells (NSHs) that are hybrid nanostructures formed by a dielectric core (such as silicon dioxide) covered by a thin and uniform layer of gold. Their optical properties have been rationalized in terms of the coupling between the plasmons of the internal and the external metal surface; the plasmon hybridization model, which can be seen as the analog of the molecular orbital theory for molecules, demonstrates that the extent of the coupling, and thus

the shift toward longer wavelengths of the LSPR, depends on the shell/core size ratio [21, 22]. These calculations are in good agreement with the experimental data.

Brinson et al. [23] in 2008 first developed a reliable multistep approach to prepare the gold NHSs. The synthesis starts from $SiO_2$ nanoparticles formed through the sol-gel method [24] and whose surface is functionalized with amino groups. Separately, gold seeds of 2–5 nm in diameter are prepared by reduction of a gold salt with an organophosphorus compound in water and then adsorbed on the amino-functionalized silica nanoparticles. With a process similar to the one described earlier for the NRDs, the further reduction of $Au^{3+}$ by formaldehyde on the seed attached to the $SiO_2$ surface allows the growth of a complete gold shell. The thickness of the metal layer and thus the position of the LSPR absorption band can be controlled by changing the amount of gold salt in the growth solution. In **Figure 2**, the extinction spectra of NSHs synthesized in our laboratory together with the corresponding TEM images are shown. Amino-functionalized $SiO_2$ nanoparticles of 120 nm were used as template for the formation of the shells. From the analysis of the TEM images, a thickness of the gold layer of 11 ± 1 nm has been measured for sample (b), which corresponded to a LSPR absorption band centered at 805 nm. When a higher concentration of gold salt was present in the growth solution, the shell thickness was increased to 20 ± 1 nm, which resulted in a surface plasmon band blue shifted to 550–600 nm (**Figure 2a**). This is explained by the increase in the distance between the inner and the outer metal layer that causes uncoupling of the two surfaces and the extinction spectrum resembles one of the clustered gold nanoparticles on silica [25]. This example illustrates the importance to achieve a strict control of the synthesis parameters in order to obtain nanoparticles with the desired properties.
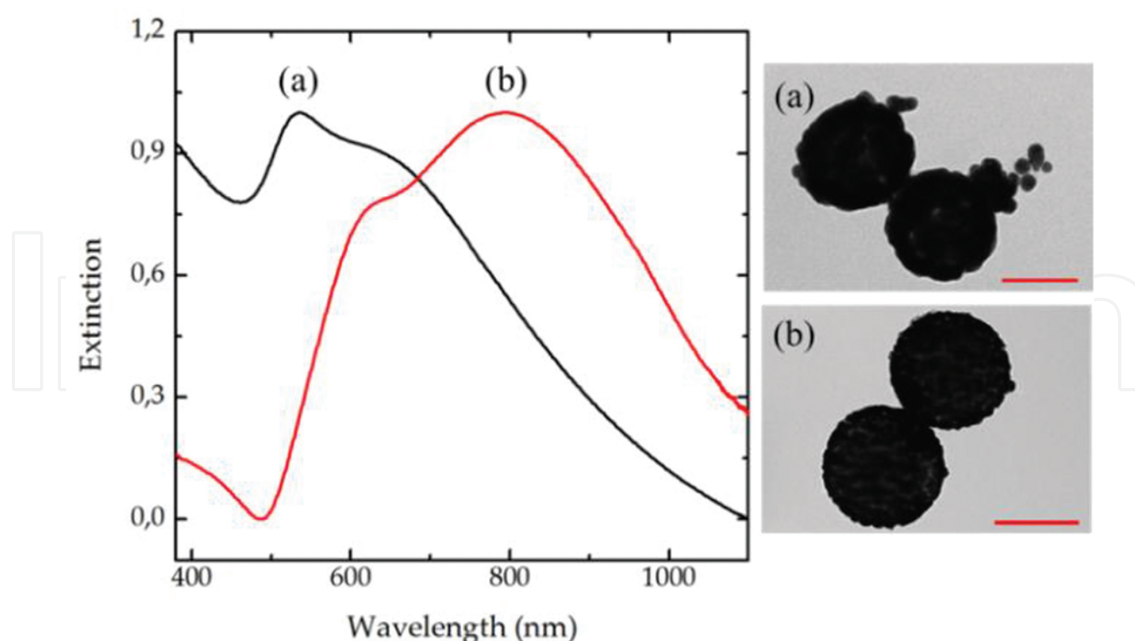


**Figure 2.** Extinction spectra of NSHs prepared with a [$Au^{3+}$] concentration in solution of (a) 39.2 μM and (b) 32.4 μM and the corresponding TEM images (scale bar = 100 nm). The amount of gold ions in solution determines the metal shell thickness and hence the position of the SPR band of the NSHs.

Recently, this multistep approach has been adapted by our group to obtain NSHs with a fluorescent core for biomedical applications [26].

## 2.3. Strategies for the surface functionalization of GNMs

The functionalization of the GNMs surface is often required for the following reasons: replacing stabilizers used for the synthesis that are toxic for the cells [27, 28], enhancing their stability in biological environments [29, 30] and introducing species (e.g., antibodies) to promote site-specific delivery of the system in the body [31, 32]. When the stabilization of the GNMs has an electrostatic nature (as for example for citrate-stabilized gold nanoparticles prepared by the common Turkevitch method [33]), the ligands can be easily substituted by stronger thiolated stabilizers under mild conditions. Using the suitable thiol linker, it is possible to functionalize the GNMs with a wide range of different species such as polymers [34, 35], fluorophores [36], deoxyribonucleic acid (DNA) [37], and antibodies [38, 39]. The ligand exchange is generally carried out at room temperature and it can also involve the use of a biphasic system [40]. However, this method has also some drawbacks. For example, the replacement of the stabilizer could be incomplete making difficult to determine the exact amount of the ligand exchanged. Also, the exchange process could lead to irreversible aggregation.

It has been shown that CTAB is toxic to the cells [41] and CTAB-coated NRDs are unstable in basic conditions [42]. However, its replacement from the surface of the gold nanorods is particularly tricky. The use of thiolate ligands usually brings to a partial exchange on the ends of the NRDs because of the preferential binding of these species on the Au {111} facets [43]. In recent years, various methods have been developed to obtain a complete CTAB removal avoiding aggregation. One of the approaches that can be used is the layer-by-layer deposition of polyelectrolytes on the CTAB-coated NRDs, which assures the control of the polymeric shell and the final surface charge of the rods. This method has been used with good results by several groups [42, 44, 45]. However, the main disadvantage is that the further functionalization of the surface with site-specific ligands is not easy to obtain. The growth of a silica shell around the nanorods is another strategy that can be adopted to remove the surfactant from the metal surface. $SiO_2$ is a good choice because it is a biocompatible material, it can be prepared with low cost and reliable methods and it can be easily functionalizable with other specific ligands. The silica coating can be carried out in a simple single-step process following the procedure first reported by Gorelikov et al. [46]. Briefly, CTAB-capped NRDs are diluted in water and NaOH is added to raise the pH to ~10. Then, the sequential addition of tetraethylorthosilicate (TEOS) as silica precursor to this solution allows the hydrolysis and condensation of the shell on the NRD surface. After mixing overnight, the silica-coated NRDs are separated from CTAB by centrifugation, removal of the supernatant and redispersion in the fresh solvent. The careful control of the TEOS-to-NRDs molar ratio in the reaction mixture and the amount of TEOS chosen for each addition determines the success of the procedure and the thickness of the coating. To demonstrate this with an example, **Figure 3** shows the extinction spectra and the TEM images of two samples of silica-coated NRDs with an aspect ratio of 2.3 prepared by our group in different experimental conditions.
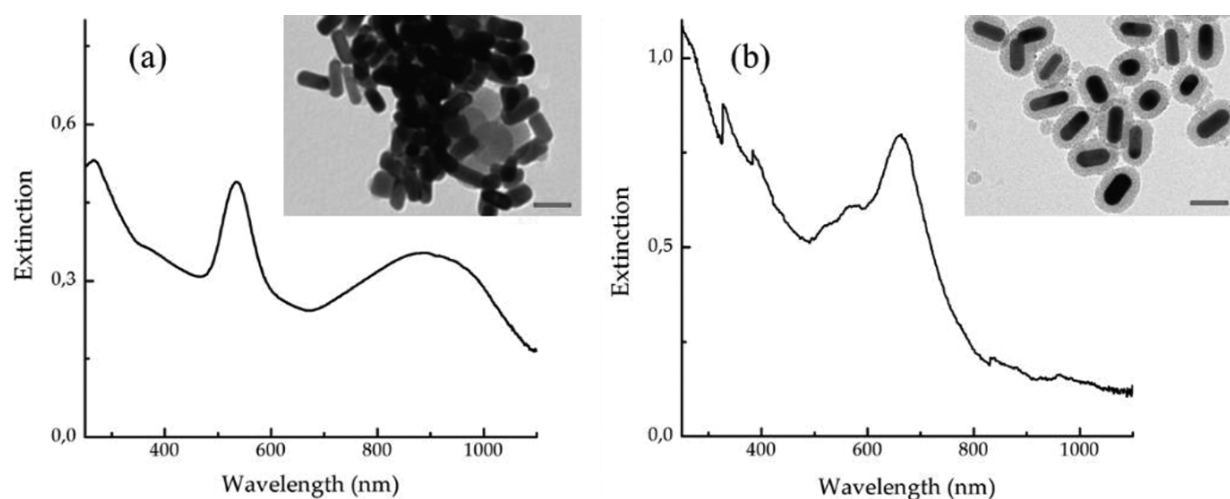
**Figure 3.** Extinction spectra of silica-coated NRDs prepared with a TEOS concentration in the solution of (a) 10.0 mM and (b) 2.3 mM together with the corresponding TEM images (scale bar = 50 nm). The growth of a homogenous silica shell is obtained by choosing the appropriate TEOS-to-NRDs molar ratio in the reaction mixture. An increase in TEOS content in solution leads to irreversible aggregation of the NRDS.

For sample (a), the coating process resulted in the aggregation of the nanorods. This aggregation is also confirmed by the extinction spectrum, which shows a broad and unstructured band with a maximum at about 900 nm that is red shifted with respect to the one of the initial CTAB-coated NRDs. For sample (b), the fine control of the experiment allowed us to obtain a homogeneous coating of the nanorods with a silica shell of 16 ± 1 nm. In this case, the extinction spectrum resembles that of the NRDs before the exchange of the stabilizer. This example also proves that the optical properties of the plasmonic nanoparticles can be successfully used to monitor the stability of the system in a fast and reliable manner during postsynthesis treatments.

## 3. Interaction of GNMs with proteins

Myoglobin (Mb) and bovine serum albumin (BSA) are used as model proteins to study the interaction with GNMs. The structure of Mb consists of a single polypeptide chain of 153 amino acids, which is arranged in eight $\alpha$-helices for about the 75% of its length. The fluorescence of Mb is dominated by the emission of its two Trp residues with one of them located at the protein surface (Trp-7) and the other one buried inside the hydrophobic pocket of protein (Trp-14). However, this emission is partially quenched by energy or electron transfer to the heme group in the protein [47] and this explains the low fluorescence quantum yield of Mb in the native form. BSA is a relatively bigger protein (583 amino acids) that has numerous biochemical functions and the most important function is the transport of drugs and fatty acids inside the body [48–50]. In analogy with Mb, it contains two Trp residues, one on the surface (Trp-134) and the other in a hydrophobic domain (Trp-212), which are responsible for the intrinsic fluorescence of the protein [51]. Modifications of the fluorescence properties of the proteins offer useful information on structural changes, rearrangements and eventually denaturation

processes occurring upon interaction with different types of chemical species [52–56]. In the following section, the same techniques have been applied to the study of GNMs-protein association.

## 3.1. Interaction of Mb with GNMs

NSHs with a silica diameter of 120 nm and a gold shell thickness of 11 nm (for morphological and optical properties refer to **Figure 2**) were gradually added to a $10^{-5}$ M aqueous solution of Mb. As shown in **Figure 4a**, the fluorescence spectrum of the protein drastically changed by interaction with the NSHs. A decrease of the band at 320 nm associated with the Trp fluorescence and the appearance of two additional emission bands centered at 390 and 440 nm were observed. Different excitation spectra were recorded at 330 and 440 nm (**Figure 4b**), demonstrating that upon interaction with NSHs two distinct emitting species become responsible of the Mb fluorescence. Time-resolved data reported in **Table 1** further supported this hypothesis. The fluorescence decay curve recorded at 330 nm for the native protein was successfully fitted with a monoexponential function giving a lifetime value of 2.6 ns. When NSHs were added to the solution of Mb, this value was reduced of about 20%.
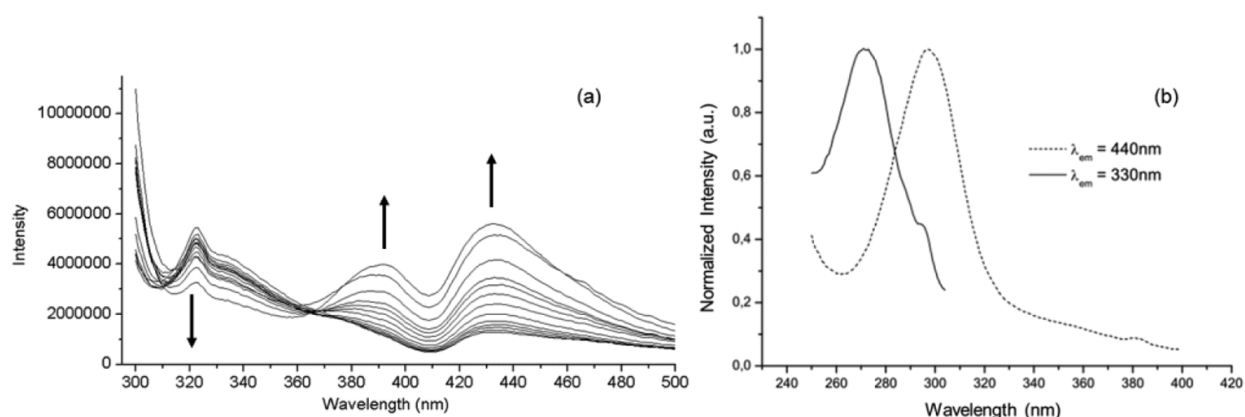


**Figure 4.** (a) Fluorescence emission spectra of Mb ($\lambda_{exc}$ = 290 nm) in the presence of increasing concentration of NSHs; (b) fluorescence excitation spectra of Mb in the presence of $2.5 \times 10^{-12}$ M NSHs recorded at two emission wavelengths. The fluorescence data indicate that a protein-nanoparticle complex is formed upon interaction of Mb with the NSHs.

The fluorescence decay signal at 390 and 440 nm showed a more complex behavior, and from the analysis of the data, we obtained two decay components of about 4.5 and 1.0–1.5 ns. These values and their relative statistical weight on the lifetime were not affected by the concentration of nanoshells in solution. All the fluorescence data suggested that the interaction of Mb with the NSHs brings to the formation of a fluorescent protein-nanoparticle complex in which the protein is in a different conformational arrangement or is partially denaturated. The value of the longer and principal component (4.5 ns) of the decay of the new species was close to the value of Trp lifetime in water [57], which would indicate that in the rearranged configuration the two Trp are more exposed to the external medium. However, the decrease in the lifetime value at 330 nm suggests that static quenching due to the formation of the Mb-NSH complex

alone cannot explain the mechanism of interaction, and energy/electron transfer processes between the Trp residues and the gold are not excluded.

| [NSHs] (M) | $\lambda_{em}$ (nm) | $\tau$ (ns) | Percentage (%) |
|---|---|---|---|
| 0 | 330 | 2.6 | 100 |
| $7.2 \times 10^{-13}$ | 330 | 2.1 | 100 |
| | 390 | 4.6 | 71.3 |
| | | 0.9 | 28.7 |
| | 440 | 4.5 | 94.3 |
| | | 1.5 | 5.7 |
| $2.5 \times 10^{-12}$ | 330 | 2.1 | 100 |
| | 390 | 4.5 | 80.5 |
| | | 0.9 | 19.5 |
| | 440 | 4.4 | 98.0 |
| | | 1.1 | 2.0 |

**Table 1.** Fluorescence decay time parameters of Mb ($\lambda_{exc}$ = 295 nm) in the presence of increasing concentration of NSHs.

The same experiment has been carried out by using CTAB-capped gold nanorods with an aspect ratio of 2.3 (**Figure 1a** for the optical and microscopy data of the sample). The addition of NRDs to a $10^{-5}$ M solution of Mb in water efficiently quenched the protein emission, but in this case, no additional bands at longer wavelengths were detected (**Figure 5a**).
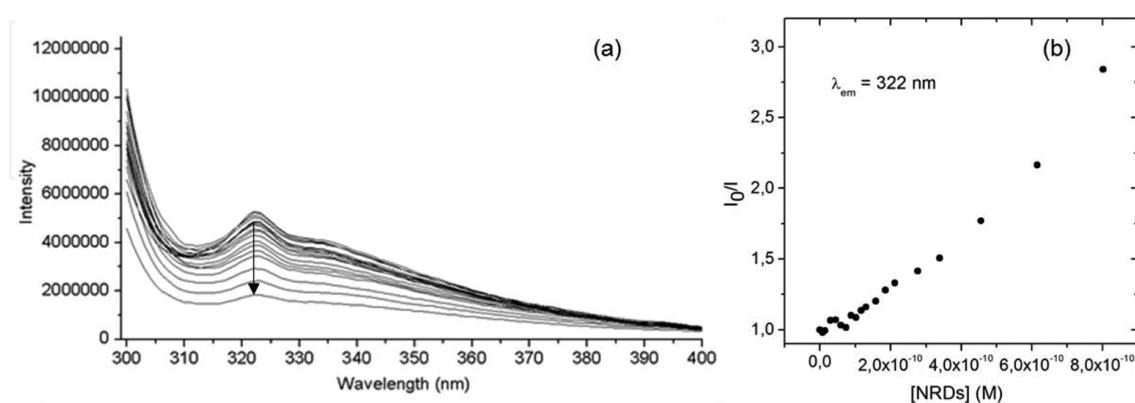


**Figure 5.** (a) Fluorescence emission spectra of Mb ($\lambda_{exc}$ = 290 nm) in the presence of increasing concentration of NRDs; (b) Stern-Volmer plot from the emission intensity values at 322 nm. The efficient quenching of the fluorescence observed upon addition of NRDs to the Mb solution demonstrates that a protein-nanoparticle complex in the ground state is formed.

One of the most used models to analyze fluorescence data is through the Stern-Volmer equation, which can give indications about the occurrence of both static and dynamic quenching processes:

$$\frac{I_0}{I} = 1 + K_{SV}[Q] = 1 + k_q \tau_0 [Q]$$

where $I_o$ and $I$ are the fluorescence intensities in the absence and in the presence of the quencher, $K_{SV}$ is the Stern-Volmer quenching constant, $k_q$ is the bimolecular quenching rate constant, $\tau_0$ is the average lifetime of the fluorophore in the absence of the quencher and [Q] is the concentration of the quencher in solution. The Stern-Volmer plot of fluorescence data (**Figure 5b**) showed a linear relationship and a $K_{SV}$ value of $1.9 \times 10^9$ M$^{-1}$ was obtained from the linear fit. Using 2.6 ns for the lifetime of the myoglobin (**Table 1**), we estimated a $k_q$ of $7.3 \times 10^{17}$ M$^{-1}$ s$^{-1}$ that is several orders of magnitude greater than the maximum dynamic collisional quenching constants of various types of quenchers with biomolecules [58]. This demonstrates that the quenching has an important static component and that a nonfluorescent Mb-NRD complex in the ground state is formed. The fluorescence measurements clearly indicate that the interaction between GNMs and the myoglobin occurs in any case through the adsorption of the proteins on the surface of the nanoparticle although with a different structural rearrangement. Different surface properties of the GNMs tuned by their size and by the nature of the stabilizers could explain these differences.

The role of the surface properties of the plasmonic NPs in the interaction with the proteins has been further investigated by using NRDs with the same aspect ratio of 2.3 in which the surfactant CTAB has been replaced by a uniform silica shell of $16 \pm 1$ nm (**Figure 3b** for the optical and morphological data of these nanoparticles).

The addition of silica-coated NRD to a $10^{-5}$ M solution of Mb brought to drastic changes in the fluorescence spectrum of the protein (**Figure 6**). The complete quenching of the emission of the native protein and the appearance of a new broad band at 365 nm was detected right after the addition of the nanoparticles. This new emission can be attributed to Trp residues that are completely exposed to a polar environment [49, 59]. The data indicate that the interaction of Mb with the NRD surface is followed by the denaturation of the protein that brings the Trp-14 to be in contact with the water solvent. The adsorption of Mb on the silica-coated nanorods has been also demonstrated by AFM microscopy. A drop of the solution containing the protein and the silica coated NRD at concentrations of $10^{-5}$ M and $5 \times 10^{-12}$ M, respectively, was deposited on freshly cleaved mica. After complete evaporation of the solvent, the sample was scanned with an AFM in tapping mode. The topographic image in **Figure 7a** shows objects of about 200–250 nm that can be associated with aggregates of 2–3 nanoparticles. The irregular surface of these particles and the presence of regions at different phase contrast (**Figure 7b**) indicate that these species are covered by Mb molecules as previously observed with microscopy techniques for other protein-silica systems studied by our group. The presence of protein molecules on the surface of the silica-coated NRDs could also assist and promote the aggregation process [60].
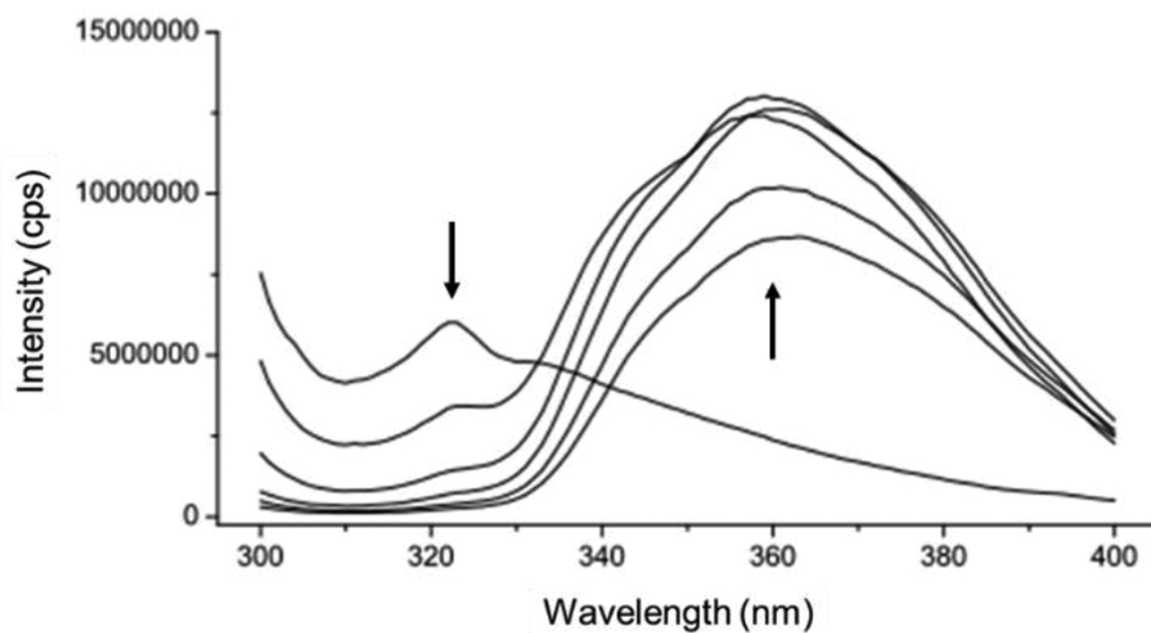
**Figure 6.** Fluorescence emission spectra of Mb ($\lambda_{exc}$ = 290 nm) in the presence of increasing concentration of silica-coated NRDs (from 0 to 6.8 × $10^{-12}$ M). The appearance of a new emission band at 365 nm is attributed to the exposure of Trp residues of Mb to the aqueous environment following the protein denaturation.
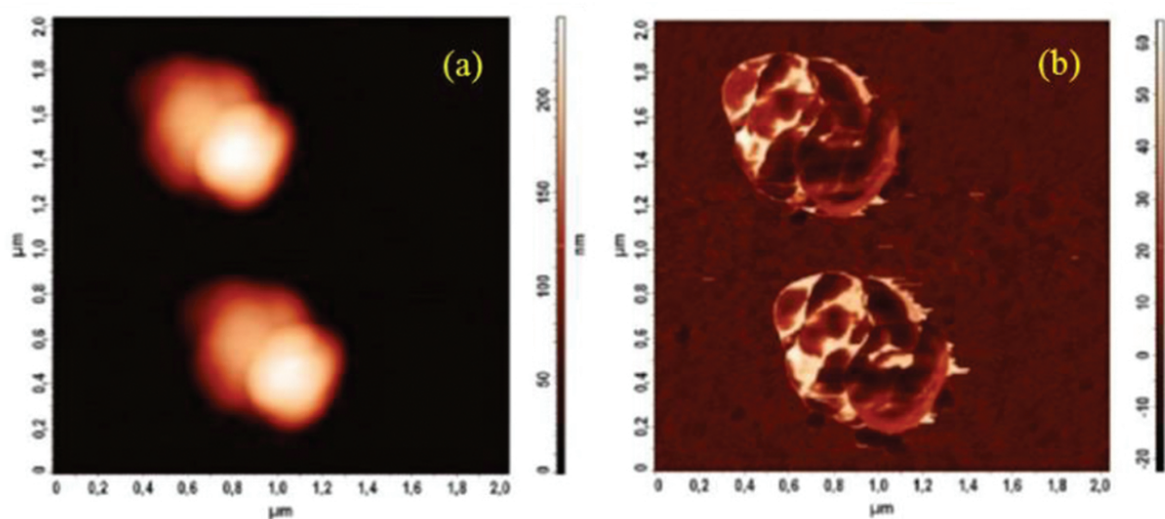


**Figure 7.** (a) Topographic and (b) phase-contrast AFM image of myoglobin and silica-coated NRDs after deposition on mica substrate. Aggregates of nanoparticles covered by myoglobin molecules are clearly observed from the images.

### 3.2. Interaction of BSA with GNMs

NRDs with different surface properties have been employed to study the interactions of plasmonic nanoparticles with BSA. The fluorescence spectra of the protein upon gradual addition of increasing amount of nanorods with an aspect ratio of 2.3 are reported in **Figure 8**.
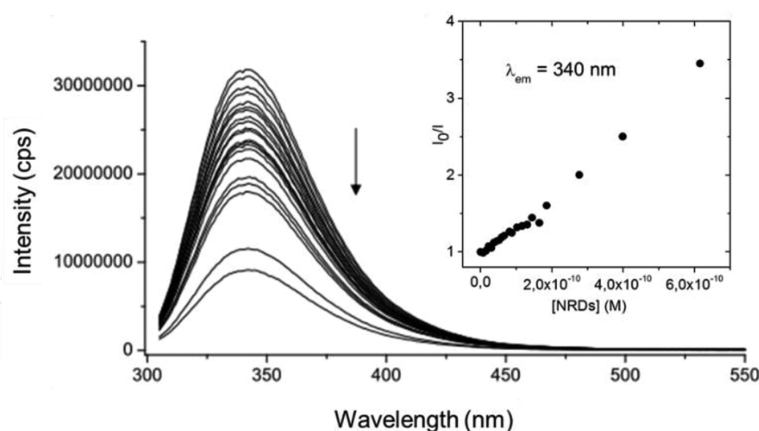
**Figure 8.** Fluorescence emission spectra of BSA ($\lambda_{exc}$ = 290 nm) in the presence of increasing concentration of NRDs; (inset) Stern-Volmer plot from the emission intensity values at 340 nm. The strong quenching of the BSA emission demonstrates the formation of nonfluorescent protein-NRD complexes.

Analogous to Mb, an efficient quenching of fluorescence was observed without any modification in the shape of the emission band. The intensity values treated with the Stern-Volmer equation showed a linear correlation of the quenching with the concentration of the NRDs added. The analysis allowed to calculate a $K_{SV}$ value of $3.9 \times 10^9$ M$^{-1}$ and a $k_q$ of $8.1 \times 10^{17}$ M$^{-1}$ cm$^{-1}$ using a calculated average lifetime of 4.8 ns for BSA. These values demonstrate once again that the interaction is dominated by static quenching, and thus, a nonfluorescent GNM-protein complex at the ground state is formed.

When a silica shell of 16 nm was grown on the NRDs replacing the surfactant, the interaction with the BSA molecules changed dramatically. In fact, as shown in **Figure 9a**, a quenching much more efficient was detected even at lower concentrations of silica-coated NRDs in solution (~$10^{-11}$–$10^{-12}$ M). Interestingly, the resulting Stern-Volmer plot (**Figure 9b**) of the data



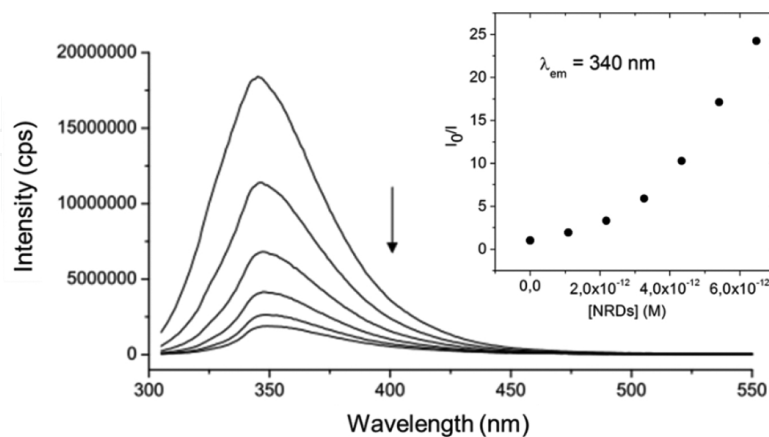**Figure 9.** Fluorescence emission spectra of BSA ($\lambda_{exc}$ = 290 nm) in the presence of increasing concentration of silica-coated NRDs; (inset) Stern-Volmer plot from the emission intensity values at 340 nm. A more complex mechanism of interaction occurs when a silica shell is grown around the nanorods interacting with the BSA molecules. This results in a more efficient quenching and an upward curvature of the Stern-Volmer plot.

showed an upward curvature which indicates that the decrease in the fluorescence intensity might be due to a bimodal mechanism of interaction. A small red shift of 2–3 of the emission maximum also suggests that a certain rearrangement of BSA follows the adsorption of the protein on the silica surface of the nanorods.

## 4. Conclusion

Nowadays, several nanodevice families are available as biomedical tools. Among them, gold-based nanomaterials have a prominent role to play because of their excellent properties. In this chapter, we demonstrated that it is possible to obtain GNMs through simple and reliable chemical methods and their optical properties can be tuned by changing the synthetic conditions. Nanorods capped with CTAB can be prepared by a seed-mediated growth method in aqueous solution and the final aspect ratio strongly affects the position of the longitudinal plasmon band of the extinction spectrum. The removal of the toxic CTAB from the metal surface of the rods is necessary in order to use these them for *in vivo* applications and we showed that different approaches can be used to exchange this surfactant with other stabilizers. By a fine control of the preparation conditions, it is possible to grow a silica shell of variable thickness on the nanorods, which can be further functionalized with site-specific ligands. Another interesting system showing plasmonic properties is gold nanoshell made of a silica core covered by a thin layer of gold. Depending on the ratio between the size of the core and the shell thickness, the surface plasmon absorption can be shifted from the visible to the NIR region of the spectrum which is desirable for biomedical applications.

In the second section, we described in detail the interaction of model proteins with these two types of gold-based nanomaterials through fluorescence and microscopy techniques. In all cases, quenching of the protein emission was detected. The data analyzed by the Stern-Volmer equation indicate that protein-nanoparticles complexes are formed at the ground state. The appearance of new red-shifted emission bands in the fluorescence spectra and the AFM images confirmed the presence of these species. The comparison between the data collected for the nanorods before and after growth of a silica shell demonstrated that the surface properties of the nanoparticles have an important role in regulating the process of protein adsorption.

The use of GNMs as biomedical devices requires the in-depth study of their therapeutic efficacy along with their potential toxicity. In this context, a deep comprehension on how the biological molecules interact with the nanoparticles is desirable. Several recent studies have been focused on the biological effects of GNMs, but a detailed description of the mechanism of interaction between proteins and nanoparticles and a comprehensive study of the factors affecting this interaction is still lacking. This knowledge would bring enormous advantages in the design of nanomaterials with controllable properties. The development of methods sensitive enough for the detailed study of NP-proteins interaction is also a challenge. For this purpose, single-molecule techniques and ultrafast spectroscopy may play a fundamental role in elucidating the mechanism of interaction between a protein and a metal surface with high spatial resolution. Moreover, a multimethod approach would allow describing in detail the process of

protein adsorption onto GNMs from different points of view. The big question that remains open is how to obtain the interaction information with a similar sensitivity in a living organism. By addressing these issues, it will be possible to create gold-based nanostructures with engineered surfaces that could interact predictably with proteins opening up the possibility to obtain more efficient therapeutic agents and nanoprobes for biomedical applications.

## Author details

Loredana Latterini[*] and Luigi Tarpani

*Address all correspondence to: loredana.latterini@unipg.it

Department of Chemistry, Biology and Biotechnology, Centro Eccellenza Materiali Innovativi Nanostrutturati (CEMIN), University of Perugia, Italy

## References

[1]  Grassian VH. When size really matters: size-dependent properties and surface chemistry of metal and metal oxide nanoparticles in gas and liquid phase environment. J Phys Chem C. 2008;112(47):18303–13. DOI: 10.1021/jp806073t

[2]  El-Sayed MA. Small is different: shape-, size-, and composition-dependent properties of some colloidal semiconductor nanocrystals. Acc Chem Res. 2004;37(5):326–33. DOI: 10.1021/ar020204f

[3]  Deng ZJ, Liang M, Monteiro M, Toth I, Minchin RF. Nanoparticle-induced unfolding of fibrinogen promotes Mac-1 receptor activation and inflammation. Nature Nanotech. 2011;6(1):39–44. DOI: 10.1038/nnano.2010.250

[4]  Simón-Vázquez R, Lozano-Fernández T, Peleteiro-Olmedo M, González-Fernández Á. Conformational changes in human plasma proteins induced by metal oxide nanoparticles. Coll Surf B: Bioint. 2014;113:198–206. DOI: 10.1016/j.colsurfb.2013.08.047

[5]  Tsai YS, Chen YH, Cheng PC, Tsai HT, Shiau AL, Tzai TS, Wu CL. TGF-β1 Conjugated to gold nanoparticles results in protein conformational changes and attenuates the biological function. Small. 2013;9(12):2119–28. DOI: 10.1002/smll.201202755

[6]  Saha K, Agasti SS, Kim C, Li X, Rotello V M. Gold nanoparticles in chemical and biological sensing. Chem Rev. 2012;112(5):2739–79. DOI: 10.1002/anie.200603735

[7]  Choi Y, Ho NH, Tung CH. Sensing phosphatase activity by using gold nanoparticles. Angew Chem Int Ed. 2007;46(5):707–9.

[8] De M, Rana S, Akpinar H, Miranda OR, Arvizo RR, Bunz UH, Rotello VM. Sensing of proteins in human serum using conjugates of nanoparticles and green fluorescent protein. Nat Chem. 2009;1(6):461–5. DOI: 10.1038/nchem.334

[9] Popovtzer R, Agrawal A, Kotov NA, Popovtzer A, Balter J, Carey TE, Kopelman R. Targeted gold nanoparticles enable molecular CT imaging of cancer. Nano Lett. 2008;8(12):4593–96. DOI: 10.1021/nl8029114

[10] Jain PK, Lee KS, El-Sayed IH, El-Sayed MA. Calculated absorption and scattering properties of gold nanoparticles of different size, shape, and composition: applications in biological imaging and biomedicine. J Phys Chem B. 2006;110(14):7238–48. DOI: 10.1021/jp057170o

[11] Li D, Teoh WY, Selomulya C, Woodward RC, Amal R, Rosche B. Flame-sprayed superparamagnetic bare and silica-coated maghemite nanoparticles: synthesis, characterization, and protein adsorption-desorption. Chem Mater. 2006;18(26):6403–13. DOI: 10.1021/cm061861v

[12] Lehman SE, Mudunkotuwa IA, Grassian VH, Larsen SC. Nano-bio interactions of porous and nonporous silica nanoparticles of varied surface chemistry: a structural, kinetic, and thermodynamic study of protein adsorption from RPMI culture medium. Langmuir. 2015;32(3):731–42. DOI: 10.1021/acs.langmuir.5b03997

[13] Calzolai L, Franchini F, Gilliland D, Rossi F. Protein–nanoparticle interaction: identification of the ubiquitin–gold nanoparticle interaction site. Nano Lett. 2010;10(8):3101–5. DOI: 10.1021/nl101746v

[14] Lundqvist M, Sethson I, Jonsson BH. Protein adsorption onto silica nanoparticles: conformational changes depend on the particles' curvature and the protein stability. Langmuir. 2004;20(24):10639–47. DOI: 10.1021/la0484725

[15] Cedervall T, Lynch I, Lindman S, Berggård T, Thulin E, Nilsson H, Dawson KA, Linse S. Understanding the nanoparticle–protein corona using methods to quantify exchange rates and affinities of proteins for nanoparticles. Proc Natl Acad Sci. 2007;104(7):2050–5. DOI: 10.1073/pnas.0608582104

[16] Link S, Mohamed M, El-Sayed M. Simulation of the optical absorption spectra of gold nanorods as a function of their aspect ratio and the effect of the medium dielectric constant. J Phys Chem B. 1999;103(16):3073–7. DOI: 10.1021/jp990183f

[17] Brioude A, Jiang X, Pileni M. Optical properties of gold nanorods: DDA simulations supported by experiments. J Phys Chem B. 2005;109(27):13138–42. DOI: 10.1021/jp0507288

[18] Ni W, Kou X, Yang Z, Wang J. Tailoring longitudinal surface plasmon wavelengths, scattering and absorption cross sections of gold nanorods. ACS Nano. 2008;2(4):677–86. DOI: 10.1021/nn7003603

[19]   Jana NR, Gearheart L, Murphy CJ. Wet chemical synthesis of high aspect ratio cylin-drical gold nanorods. J Phys Chem B. 2001;105(19):4065–7. DOI: 10.1021/jp0107964

[20]   Nikoobakht B, El-Sayed MA. Preparation and growth mechanism of gold nanorods (NRs) using seed-mediated growth method. Chem Mater. 2003;15(10):1957–62. DOI: 10.1021/cm020732l

[21]   Prodan E, Radloff C, Halas NJ, Nordlander P. A hybridization model for the plasmon response of complex nanostructures. Science. 2003;302(5644):419–22. DOI: 10.1126/science.1089171

[22]   Jain PK, El-Sayed MA. Universal scaling of plasmon coupling in metal nanostructures: extension from particle pairs to nanoshells. Nano Lett. 2007;7(9):2854–8. DOI: 10.1021/nl071496m

[23]   Brinson BE, Lassiter JB, Levin CS, Bardhan R, Mirin N, Halas NJ. Nanoshells made easy: improving Au layer growth on nanoparticle surfaces. Langmuir. 2008;24(24):14166–71. DOI: 10.1021/la802049p

[24]   Stöber W, Fink A, Bohn E. Controlled growth of monodisperse silica spheres in the micron size range. J Coll Interf Sci. 1968;26(1):62–9. DOI: 10.1016/0021-9797(68)90272-5

[25]   Westcott SL, Oldenburg SJ, Lee TR, Halas NJ. Construction of simple gold nanoparticle aggregates with controlled plasmon–plasmon interactions. Chem Phys Lett. 1999;300(5):651–5. DOI: 10.1016/S0009-2614(98)01410-9

[26]   Latterini L, Tarpani L. Hierarchical assembly of nanostructures to decouple fluores-cence and photothermal effect. J Phys Chem C. 2011;115(43):21098–104. DOI: 10.1021/jp208124x

[27]   Alkilany AM, Nagaria PK, Hexel CR, Shaw TJ, Murphy CJ, Wyatt MD. Cellular uptake and cytotoxicity of gold nanorods: molecular origin of cytotoxicity and surface effects. Small. 2009;5(6):701–8. DOI: 10.1002/smll.200801546

[28]   Rayavarapu RG, Petersen W, Hartsuiker L, Chin P, Janssen H, Van Leeuwen FW, Otto C, Manohar S, Van Leeuwen TG. In vitro toxicity studies of polymer-coated gold nanorods. Nanotechnology. 2010;21(14):145101. DOI: 10.1088/0957-4484/21/14/145101

[29]   Chompoosor A, Han G, Rotello VM. Charge dependence of ligand release and mono-layer stability of gold nanoparticles by biogenic thiols. Bioconj Chem. 2008;19(7):1342–45. DOI: 10.1021/bc8000694

[30]   Rosi NL, Giljohann DA, Thaxton CS, Lytton-Jean AK, Han MS, Mirkin CA. Oligonu-cleotide-modified gold nanoparticles for intracellular gene regulation. Science. 2006;312(5776):1027–30. DOI: 10.1126/science.1125559

[31]   Leduc C, Si S, Gautier J, Soto-Ribeiro M, Wehrle-Haller B, Gautreau A, Giannone G, Cognet L, Lounis B. A highly specific gold nanoprobe for live-cell single-molecule imaging. Nano Lett. 2013;13(4):1489–94. DOI: 10.1021/nl304561g

[32] Black KC, Yi J, Rivera JG, Zelasko-Leon DC, Messersmith PB. Polydopamine-enabled surface functionalization of gold nanorods for cancer cell-targeted imaging and photothermal therapy. Nanomedicine. 2013;8(1):17–28. DOI: 10.2217/nnm.12.82

[33] Turkevich J, Stevenson PC, Hillier J. A study of the nucleation and growth processes in the synthesis of colloidal gold. Discuss Faraday Soc. 1951;11:55–75. DOI: 10.1039/DF9511100055

[34] Corbierre MK, Cameron NS, Lennox RB. Polymer-stabilized gold nanoparticles with high grafting densities. Langmuir. 2004;20(7):2867–73. DOI: 10.1021/la0355702

[35] Boca SC, Astilean S. Detoxification of gold nanorods by conjugation with thiolated poly (ethylene glycol) and their assessment as SERS-active carriers of Raman tags. Nanotechnology. 2010;21(23):235601. DOI: 10.1088/0957-4484/21/23/235601

[36] Nerambourg N, Werts MH, Charlot M, Blanchard-Desce M. Quenching of molecular fluorescence on the surface of monolayer-protected gold nanoparticles investigated using place exchange equilibria. Langmuir. 2007;23(10):5563–70. DOI: 10.1021/la070005a

[37] Zhang X, Servos MR, Liu J. Instantaneous and quantitative functionalization of gold nanoparticles with thiolated DNA using a pH-assisted and surfactant-free route. J Am Chem Soc. 2012;134(17):7266–9. DOI: 10.1021/ja3014055

[38] Behnke T, Mathejczyk JE, Brehm R, Würth C, Gomes FR, Dullin C, Napp J, Alves F, Resch-Genger U. Target-specific nanoparticles containing a broad band emissive NIR dye for the sensitive detection and characterization of tumor development. Biomaterials. 2013;34(1):160–70. DOI: 10.1016/j.biomaterials.2012.09.028

[39] Joshi PP, Yoon SJ, Hardin WG, Emelianov S, Sokolov KV. Conjugation of antibodies to gold nanorods through Fc portion: synthesis and molecular specific imaging. Bioconj Chem. 2013;24(6):878–88. DOI: 10.1021/bc3004815

[40] Warner MG, Reed SM, Hutchison JE. Small, water-soluble, ligand-stabilized gold nanoparticles synthesized by interfacial ligand exchange reactions. Chem Mater. 2000;12(11):3316–20. DOI: 10.1021/cm0003875

[41] Connor EE, Mwamuka J, Gole A, Murphy CJ, Wyatt MD. Gold nanoparticles are taken up by human cells but do not cause acute cytotoxicity. Small. 2005;1(3):325–7. DOI: 10.1002/smll.200400093

[42] Ding H, Yong KT, Roy I, Pudavar HE, Law WC, Bergey EJ, Prasad PN. Gold nanorods coated with multilayer polyelectrolyte as contrast agents for multimodal imaging. J Phys Chem C. 2007;111(34):12552–7. DOI: 10.1021/jp0733419

[43] Chang JY, Wu H, Chen H, Ling YC, Tan W. Oriented assembly of Au nanorods using biorecognition system. Chem Comm. 2005;(8):1092–4. DOI: 10.1039/B414059A

[44] Huang HC, Barua S, Kay DB, Rege K. Simultaneous enhancement of photothermal stability and gene delivery efficacy of gold nanorods using polyelectrolytes. ACS Nano. 2009;3(10):2941–52. DOI: 10.1021/nn900947a

[45] Kirui DK, Krishnan S, Strickland AD, Batt CA. PAA-derived gold nanorods for cellular targeting and photothermal therapy. Macromol Biosci. 2011;11(6):779–88. DOI: 10.1002/mabi.201100050

[46] Gorelikov I, Matsuura N. Single-step coating of mesoporous silica on cetyltrimethyl ammonium bromide-capped nanoparticles. Nano Lett. 2008;8(1):369–73. DOI: 10.1021/nl0727415

[47] Consani C, Auböck G, Van Mourik F, Chergui M. Ultrafast tryptophan-to-heme electron transfer in myoglobins revealed by UV 2D spectroscopy. Science. 2013;339(6127):1586–9. DOI: 10.1126/science.1230758

[48] Du C, Deng D, Shan L, Wan S, Cao J, Tian J, Achilefu S, Gu Y. A pH-sensitive doxorubicin prodrug based on folate-conjugated BSA for tumor-targeted drug delivery. Biomaterials. 2013;34(12):3087–97. DOI: 10.1016/j.biomaterials.2013.01.041

[49] Burstein E, Vedenkina N, Ivkova M. Fluorescence and the location of tryptophan residues in protein molecules. Photochem Photobiol. 1973;18(4):263–79. DOI: 10.1111/j.1751-1097.1973.tb06422.x

[50] Bhushan B, Dubey P, Kumar SU, Sachdev A, Matai I, Gopinath P. Bionanotherapeutics: niclosamide encapsulated albumin nanoparticles as a novel drug delivery system for cancer therapy. RSC Adv. 2015;5(16):12078–86. DOI: 10.1039/C4RA15233F

[51] Peters T. Serum albumin. Adv Prot Chem. 1985;37:161–245.

[52] Naik P, Chimatadar S, Nandibewoor S. Interaction between a potent corticosteroid drug–dexamethasone with bovine serum albumin and human serum albumin: a fluorescence quenching and fourier transformation infrared spectroscopy study. J Photochem Photobiol B Biol. 2010;100(3):147–59. DOI: 10.1016/j.jphotobiol.2010.05.014

[53] Kandagal P, Ashoka S, Seetharamappa J, Shaikh S, Jadegoud Y, Ijare O. Study of the interaction of an anticancer drug with human and bovine serum albumin: spectroscopic approach. J Pharm Biomed Anal. 2006;41(2):393–9. DOI: 10.1016/j.jpba.2005.11.037

[54] Tian J, Liu J, Tian, X, Hu Z, Chen X. Study of the interaction of kaempferol with bovine serum albumin. J Mol Struct. 2004;691(1):197–202. DOI: 10.1016/j.molstruc.2003.12.019

[55] Zhou J, Wu X, Yang C, Gu X, Zhou L, Song K, Feng Y, Shen J. Spectroscopic studies on the interaction of hypocrellin A with myoglobin. J Spectros. 2007;21(4):235–43. DOI: 10.1155/2007/503537

[56] Giugliarelli A, Tarpani L, Latterini L, Morresi A, Paolantoni M, Sassi P. Spectroscopic and microscopic studies of aggregation and fibrillation of lysozyme in water/ethanol solutions. J Phys Chem B. 2015;119(41):13009–17. DOI: 10.1021/acs.jpcb.5b07487

[57] Grinvald A, Steinberg I. The fluorescence decay of tryptophan residues in native and denatured proteins. BBA-Protein Struct. 1976;427(2):663–78. DOI: 10.1016/0005-2795(76)90210-5

[58] Lakowicz JR. (2013) Principles of fluorescence spectroscopy. Berlin: Springer. DOI: 10.1007/978-0-387-46312-4

[59] Vivian JT, Callis PR. Mechanisms of tryptophan fluorescence shifts in proteins. Biophys J. 2001;80(5):2093–109. DOI: 10.1016/S0006-3495(01)76183-8

[60] Latterini L, Tarpani L. (2012) AFM measurements to investigate particulates and their interactions with biological macromolecules. In Atomic force microscopy investigations into biology - from cell to protein. Rijeka: Intech. DOI: 10.5772/2092